AIP Advances

Metamaterial-based dual-band microwave absorber with polarization insensitive and wide-angle performance

Cite as: AIP Advances **8**, 095016 (2018); https://doi.org/10.1063/1.5020702
Submitted: 26 December 2017 . Accepted: 04 September 2018 . Published Online: 14 September 2018

Mayank Agarwal, and Manoj Kumar Meshram

AIP ADVANCES **8**, 095016 (2018)

Metamaterial-based dual-band microwave absorber with polarization insensitive and wide-angle performance

Mayank Agarwal and Manoj Kumar Meshram[a]
Department of Electronics Engineering, Indian Institute of Technology (Banaras Hindu University), Varanasi, U.P. 221 005, India

(Received 26 December 2017; accepted 4 September 2018; published online 14 September 2018)

A polarization insensitive, wide angle low profile metamaterial absorber with dual-band absorption characteristics in C- and X-frequency bands is presented in this paper. The parametric variation is discussed in details to understand the dependence of absorption frequency and absorption level on the design parameters. The proposed structure supports the realization of near unity absorption at the two absorption frequencies independently by suitably varying the design parameters. The absorption mechanism is explained with the *E*-field and surface current distribution plots at the peak absorption frequencies. The absorption is due to the simultaneous excitation of electric and magnetic resonance in the structure. Constitutive electromagnetic parameters of the proposed structure are also retrieved and plotted against frequency. A sample of the proposed absorber is fabricated and measured response validates the numerical results. https://doi.org/10.1063/1.5020702

I. INTRODUCTION

The requirement of having the alternatives of conventional microwave absorbers[1–6] led to the development of electromagnetically engineered absorbers popularly known as metamaterial absorber. Conventional microwave absorbers need to be replaced in the applications that require lightweight, low profile and low-cost absorbing materials. Such applications include radar cross section reduction,[7] mutual coupling reduction in antenna arrays,[8] stealth technology,[9] electromagnetic compatibility[10] and many more. Metamaterial absorbers suitably fit in these applications with the added advantage of frequency tunability over a wide frequency range by just varying the design parameters. Polarization insensitive nature and wide angle performance are the desired characteristics of such absorber structures.

Several metamaterial absorber structures with near unity absorption in the X-frequency band are presented in the literature.[11–13] Designing the structure with the small footprint for low GHz frequency range puts a challenge.[14] Moreover, multiband/wideband absorption responses are also in great demand. A pattern of consecutive unit cells with varying dimensions and/or multilayer structure are realized for achieving multiband/wideband absorption characteristics.[15,16] However, a single unit cell designed to have the multiband response is preferred due to its small profile. Such single unit cells are realized for dual-band absorbance in terahertz domain.[17,18]

In this paper, an ultra-thin wide-angle polarization-insensitive metamaterial unit cell is proposed to achieve dual-band absorbance in the microwave frequency domain. Two distinct absorption frequencies one each in C- and X-band are obtained by suitably combining the basic geometries of the closed ring resonator and the patch in a single unit cell. The two geometries provide different absorption frequencies individually (3.135 GHz by the CRR and 7.275 by the patch). While on combining these geometries in a single unit cell, the field induced due to the incident wave on the individual

[a]mkmeshram.ece@iitbhu.ac.in

geometries get perturbed. Therefore, the absorption frequencies in the resultant structure get shifted and the two absorption frequencies one each in C- and X-band is obtained. Square-shaped closed ring resonator is employed as resonator along with a square patch attached inside it with diagonal strips. Identical absorption characteristics for TE and TM polarized incident wave is obtained due to the four-fold symmetry present in the structure.[19–21] The design schematic and its absorption response are presented in section II. The dependence of the absorption frequency and absorption level on the design parameters of the proposed structure is discussed in detail in section III. Absorption mechanism of the proposed absorber is discussed with the help of *E*-field and surface current distribution plots in section IV. Wide angle performance is presented in section V. In section VI, the electromagnetic parameters of the proposed structure are retrieved using electric and magnetic susceptibilities. A prototype of the proposed absorber is fabricated and is experimentally verified by free space measurement method. The comparison of the measured and simulated responses is presented in section VII and is found in close agreement. Polarization-insensitive behaviour of the proposed absorber is also discussed in this section. The performance comparison of the proposed absorber with some other reported dual-band absorbers is presented in section VIII.

II. DESIGN OF THE STRUCTURE AND ABSORPTION RESPONSE

The unit cell of the proposed absorber consists of a dielectric layer sandwiched between the two metallic layers as shown in Fig. 1(a). FR-4 glass epoxy (ε_r = 4.4, $tan\delta$ = 0.02) with a thickness of 0.8 mm is used as the dielectric substrate. The top metallic layer is an electric resonator and a complete metallic plane is present at the bottom layer. Metallic layers are constructed of 35 µm thick copper with a finite conductivity of 5.8 x 10^7 S/m. The geometry of the electric resonator is presented in Fig. 1(b) along with detailed dimensions, and is placed in *xy*-plane. The proposed unit cell is designed and analyzed using periodic boundary conditions along *x*- and *y*-direction in CST Microwave Studio. Plane wave modes (TE(0, 0) and TM(0, 0)) are injected into the proposed unit cell from *z*-direction using floquet port excitation in the numerical solver. In TE(0, 0) mode, *E*-field is polarized along *y*-axis while the orientation of *E*-field is along the *x*-axis in TM(0, 0) mode. The electric resonator consists of a square-shaped ring with a square patch enclosed in it and the two are connected by the diagonal strips. The optimization of the geometric parameters of the resonator adjust the corresponding inductances and capacitances, and hence the absorption frequency. Since capacitance in the structure also depends on the substrate permittivity and thickness, therefore, these

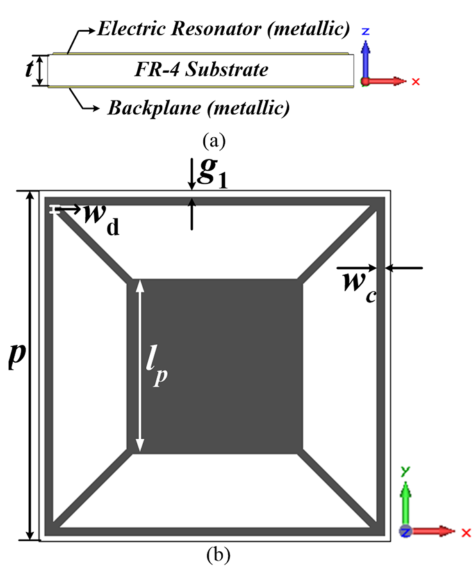

FIG. 1. (a) Side view, and (b) top view of the unit cell of the proposed absorber structure (Dimensions: p = 12 mm, g_1 = 0.2 mm, w_d = 0.2 mm, l_p = 6 mm, w_c = 0.3 mm, t = 0.8 mm).

parameters also affect the absorption frequency.[22] The level of absorption is determined by the ohmic losses provided by the resonator resistance and the dielectric losses which mainly depend on the dielectric loss tangent and thickness of the dielectric material.

The presence of complete metallic backplane reduces the transmittivity ($|S_{21}(\omega)|^2$, 1 and 2 denote the ports above the top metallic layer and below the metallic backplane, respectively) of the structure to zero. The absorption of the structure is then calculated using (1).

$$A(\omega) = 1 - |S_{11}(\omega)|^2 \tag{1}$$

where, $S_{11}(\omega)$ is the reflection coefficient of the structure. Therefore, the reflected power needs to be minimized for obtaining maximum absorption. The reflection and absorption characteristics of the proposed structure are presented in Fig. 2(a). Maximum absorption of 95.02% and 99.84% are obtained at 4.215 GHz and 10.95 GHz, respectively for normal incidence of the wave. It is also observed that identical absorption characteristics are obtained for the TE and TM polarization.

The general form of the normalized input impedance is as presented in (2). At the frequency of absorption, $Im(Z)$ should be zero. $Re(Z)$ should be close to unity for perfect matching of the input impedance of the structure with free space impedance, so that reflection from the structure gets minimized and power of the incident wave completely transfer into the structure. The coupled power gets dissipated owing to the ohmic and dielectric losses of the structure. The normalized input impedance (Z) of the proposed structure is calculated using (3) and is presented in Fig. 2(b). In (3), $|S_{21}| = 0$ is considered due to the complete metallic backplane on the bottom side of the substrate. The obtained values of normalized input impedance are 1.57-j0.04 and 1.07+j0.04 at 4.215 GHz and 10.95 GHz, respectively. It is observed that the $Re(Z)$ of the structure at the first absorption frequency is higher than that of the free space impedance due to which significant reflection loss occurs and

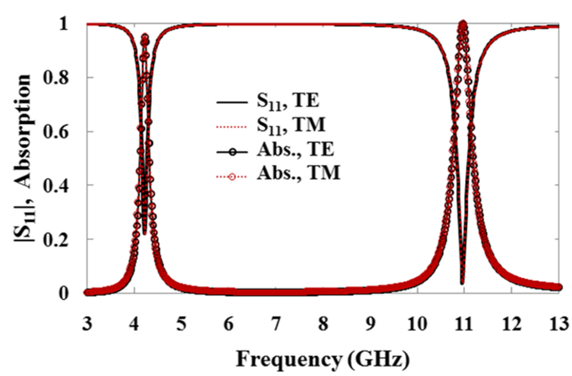

(a)

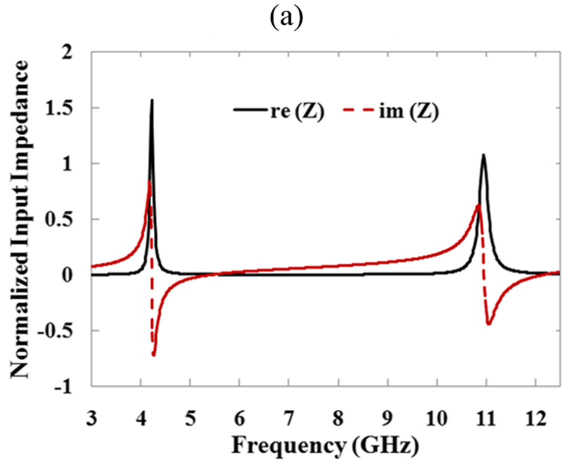

(b)

FIG. 2. (a) Reflection coefficient and absorption characteristics and (b) normalized input impedance of the proposed structure.

absorptivity reduces by 4.98% at 4.215 GHz, however, at 10.95 GHz near-perfect absorption (∼100%) is obtained.

$$Z = Re(Z) + jIm(Z) \tag{2}$$

$$Z = \sqrt{\frac{(1+S_{11})^2 - S_{21}^2}{(1-S_{11})^2 - S_{21}^2}} = \frac{1+S_{11}}{1-S_{11}} \tag{3}$$

III. OPTIMIZATION OF THE ABSORPTION FREQUENCY AND ABSORPTION LEVEL

The absorption frequency is optimized by varying the geometrical parameters of the structure. The variation in the geometrical parameters changes the inductance (L) and capacitance (C) associated with the structure. The reflection response of the proposed unit cell under the variation of various geometrical parameters is presented in Fig. 3(a)–(e). It is noted that at a time only one parameter is varying while all other parameters kept constant. It is observed from Fig. 3(a) that increase in the cell periodicity 'p' brings both the absorption frequencies towards lower frequency side. With the

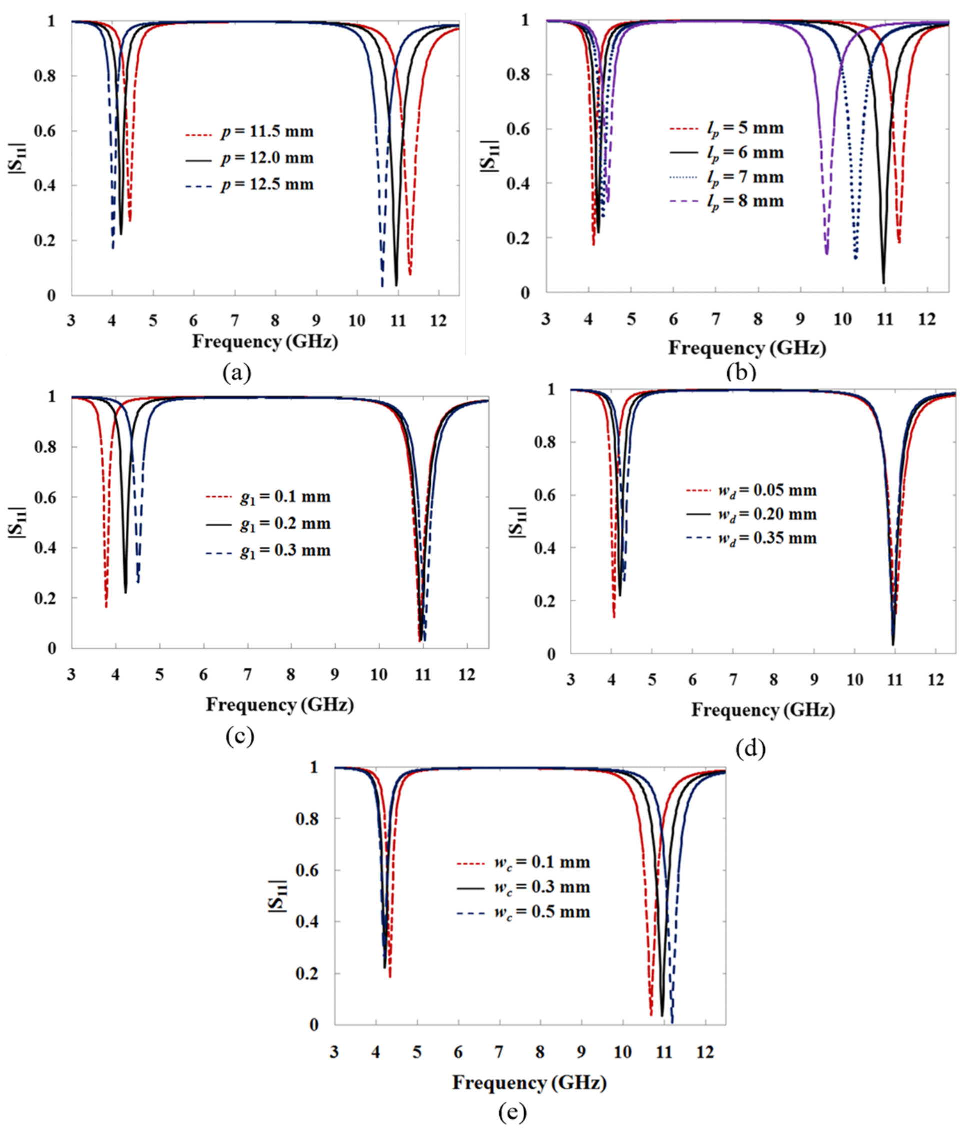

FIG. 3. Effect of varying (a) 'p' (b) 'l_p' (c) 'g_1' (d) 'w_d' (e) 'w_c' on the reflection characteristics.

increase in 'p', the length of CRR and diagonal arms increases, which increases the overall inductance of the structure and hence, resonant frequencies decreases. The increase in patch length 'l_p' increases the first absorption frequency (see Fig. 3(b)). With the increase in patch length, diagonal arm length reduces which reduces the overall path of the surface current at first absorption frequency and hence frequency increases. It is further observed that increase in 'l_p' decreases the second absorption frequency and it is due to the increase in patch capacitance. Fig. 3(c) and (d) shows that the increase in 'g_1' and 'w_d' shifts the first absorption frequency towards the higher frequency side keeping second absorption frequency almost constant. With the increase in 'g_1', CRR length reduces and the gap between two consecutive unit cell increases which reduces the associated inductance and capacitance, respectively. Therefore, the absorption frequency shifts towards higher frequency side. The increase in 'w_d' increases the width of the diagonal arm, which reduces the associated inductance and hence absorption frequency increases. The effect of varying CRR width 'w_c' is shown in Fig. 3(e), and it is observed that increase in 'w_c' increases the second absorption frequency without significantly affecting the first absorption frequency. It is noted from the unit cell schematic that on increasing 'w_c' the diagonal arm length also reduces, which in turn reduces the associated inductance. At the first absorption frequency, the effect of the decrease in inductance is counterbalanced by the increase in capacitance due to the increase in width of the CRR. Therefore, the LC product remains same keeping first absorption frequency almost constant. Moreover, the reduction in inductance increases the second absorption frequency. It is further observed that the absorption level remains above 90% in almost all the cases. Hence, by suitably varying these geometrical parameters, both the absorption frequencies can be tuned independently.

The reflection characteristics of the proposed structure with varying substrate thickness (t) are presented in Fig. 4. The first absorption frequency decreases with the increase of 't' while second absorption frequency is almost unaffected. With the increase in substrate thickness capacitance decreases while associated inductance values increases. Since first absorption frequency is mainly due to the excitation of the square loop which has the high value of inductance owing to the smaller width and hence, increases in inductance is much greater in value compared to decrease in capacitance. Therefore, LC product increases effectively causing the frequency to shift to the lower side of the spectrum. The second absorption frequency is mainly determined by the excitation of the square patch and owing to the large width of the patch corresponding inductance value is smaller and comparable to the associated capacitance, and hence decrease in capacitance is counterbalanced by the increase in inductance keeping LC product almost constant.

The absorption frequency also depends on the permittivity of the substrate materials. To better understand this dependence, the proposed absorber structure is considered as being constructed of microstrip lines of various width. The quasi-static analysis of the microstrip line explains that

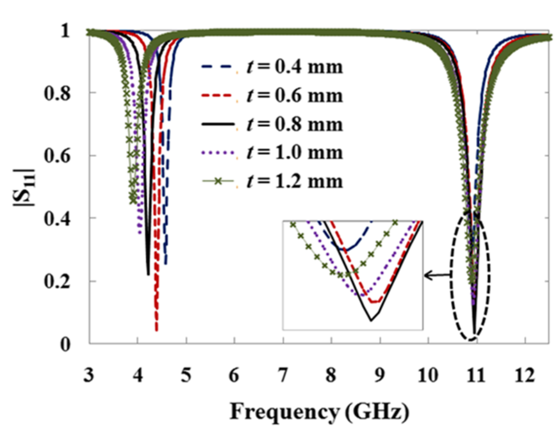

FIG. 4. Effect of varying substrate thickness 't' on the reflection characteristics (see inset for the zoomed view of response at second absorption frequency).

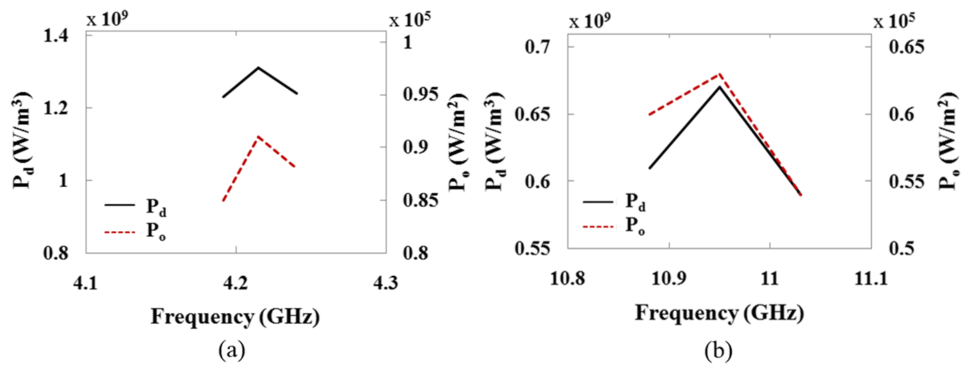

FIG. 5. Dielectric power loss density and surface power loss density for the (a) first absorption band and (b) second absorption band.

the capacitance of the microstrip line is directly proportional to its effective dielectric constant.[23] Therefore, with the increase in permittivity of the substrate material, capacitance increases, and frequency decreases.

At the frequency of absorption, $Im(Z)$ becomes equal to zero and the level of absorption is determined by the $Re(Z)$. $Re(Z)$ mainly depends on the ohmic and dielectric losses present in the structure (the effect of the real part of the complex input impedance of the grounded lossy dielectric is negligible).[24] Fig. 5 presents the simulated power loss density (volume) representing dielectric losses and surface power loss density representing ohmic losses in the 90% absorption bands. It is observed that the ohmic losses are about the fourth order of magnitude lower than that of the dielectric losses. Therefore, the effect of ohmic losses on the absorption level is neglected which is also consisted of the result presented in Ref. 25. Now the dielectric losses are the only parameter which needs to be investigated for in-depth analysis of the absorption level. The dielectric losses mainly depend on the thickness and the loss tangent of the dielectric material used.

The thickness of the substrate plays a dominant role in deciding the absorption level. It is observed from Fig. 4 that the reflection response is a monotone function of substrate thickness. The reflection coefficient decreases and reaches its minimum value then increases further with the increase of substrate thickness. Hence, there will always be an optimum value of thickness at which reflection becomes minimum. For its better understanding, the real part of the normalized impedance (Z) of the structure is plotted against frequency for various substrate thickness in Fig. 6. It is observed that the $Re(Z)$ first increases up to unity for t = 0.6 mm at first absorption frequency and for t = 0.8 mm at second absorption frequency and then $Re(Z)$ go away from unity again. The optimization of the proposed structure is carried out with the substrate thickness of 0.8 mm owing to its availability.

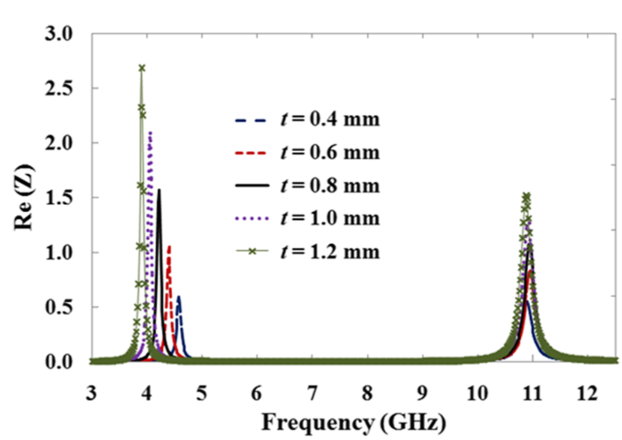

FIG. 6. Effect of varying substrate thickness 't' on the $Re(Z)$ of the structure.

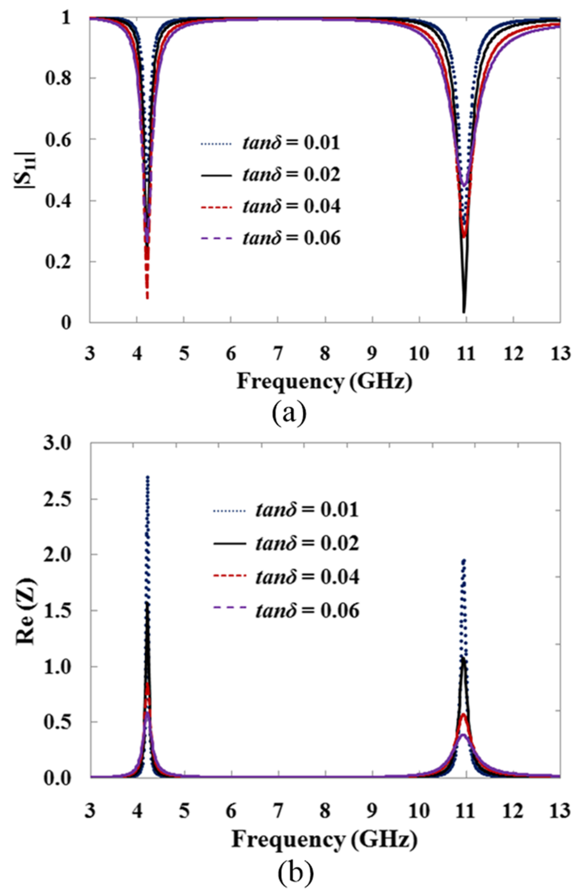

FIG. 7. Effect of varying dielectric loss tangent '*tanδ*' by keeping ε_r constant (ε_r = 4.4) on the (a) reflection characteristics, and (b) *Re*(*Z*) of the structure.

The variation in the dielectric loss tangent (*tanδ*) by keeping the real part of the permittivity constant does not affect the absorption frequency as shown in Fig. 7(a). The absorption level is a monotone function of *tanδ*. It is observed from Fig. 7(b) that the real part of the input impedance decreases with the increase of *tanδ*, and it becomes unity at a specific value of *tanδ* only.

IV. ABSORPTION MECHANISM

At the frequencies of absorption, reflection (due to perfect matching of structure impedance with free space impedance) and transmission (due to complete metallic backplane) become zero and hence the absorption of the structure become 100%. The coupling of the energy of the incident wave to the structure takes place due to the simultaneous excitation of electric and magnetic resonances in the structure.

The electric field distribution and surface current distribution for the TE polarized normally incident wave at the frequencies of absorption are presented in Fig. 8(a) and (b), respectively. The plot in Fig. 8(a) shows how the energy associated with the electrical component of incident wave transfers to the resonator at the absorption frequencies. The electrical energy is mainly confined to the loop and diagonal arms at the first absorption frequency while in the patch and diagonal arms at the second absorption frequency. Fig. 8(b) presents the surface current at the top and bottom metallic layers and it is observed that the current in the two layers is anti-parallel. Therefore, current loops are formed in between the two layers in a direction perpendicular to the incident magnetic field. This leads to the generation of magnetic resonance and energy associated with the incident magnetic field couples to the structure.

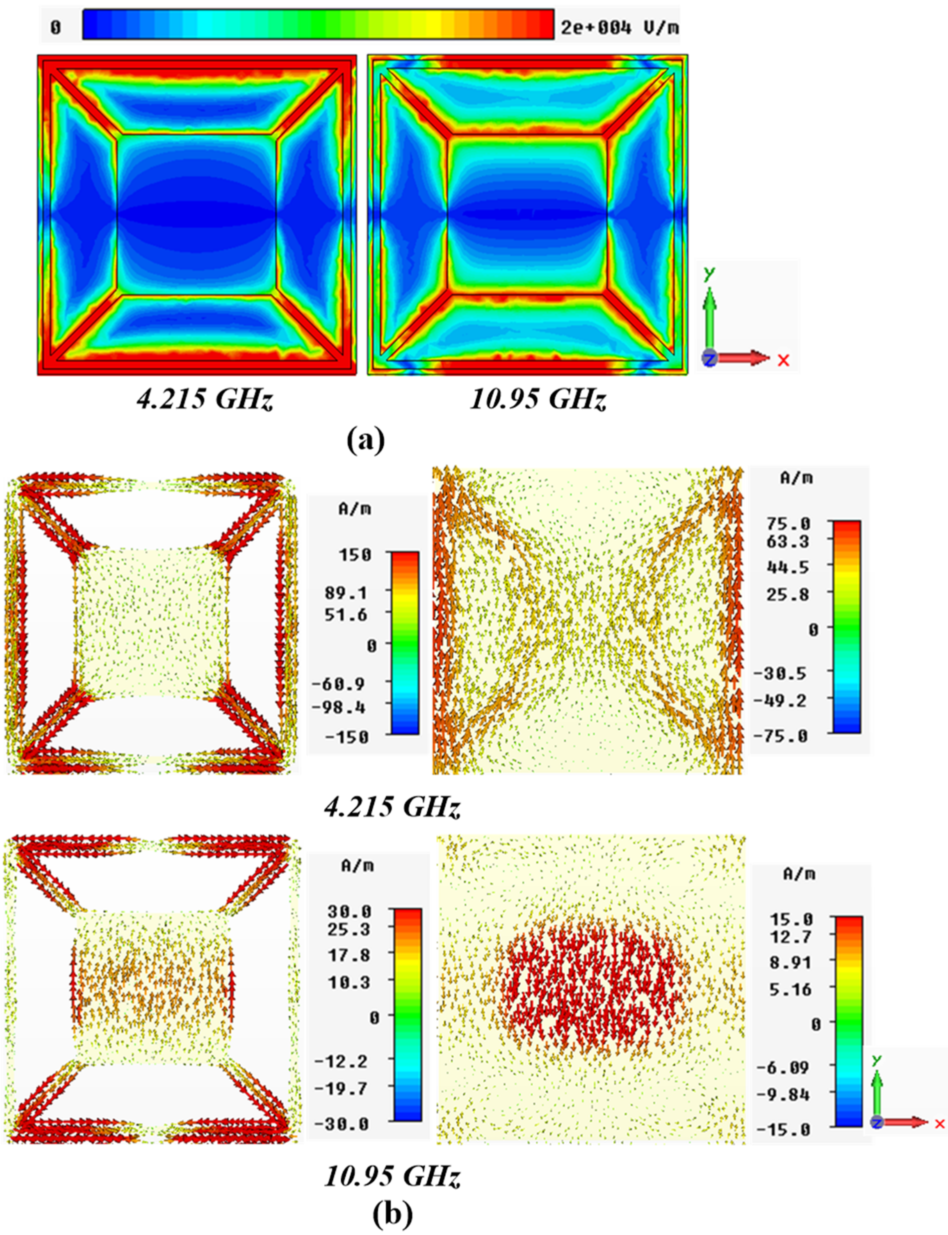

FIG. 8. (a) E-field distributions and (b) surface current distributions on the top and bottom layers of the proposed absorber at the peak absorption frequencies.

V. WIDE-ANGLE PERFORMANCE

The wide angle performance of the proposed structure is investigated for the TE and TM polarized incident wave in Fig. 9(a) and (b), respectively. For TE polarized case, the plane containing the propagation vector (k) and H-vector is rotated by the incidence angle 'θ' keeping the direction of E-vector constant. For TM polarized case, the k-E plane is rotated by the incidence angle 'θ' keeping the direction of H-vector constant. It is observed that in both the cases the two absorption frequencies remain almost the same (with a variation of less than 5%). However, the absorptivity (calculated using (1)) decreases beyond a certain value of 'θ'. For TE polarized incident wave, absorptivity is better than 95% up to 60^0 and better than 96% up to 45^0 for the first and second absorption frequency, respectively. For TM polarized incident wave, absorptivity is better than 92% up to 45^0 and better than 99% up to 60^0 for the first and second absorption frequency, respectively. Thus, the

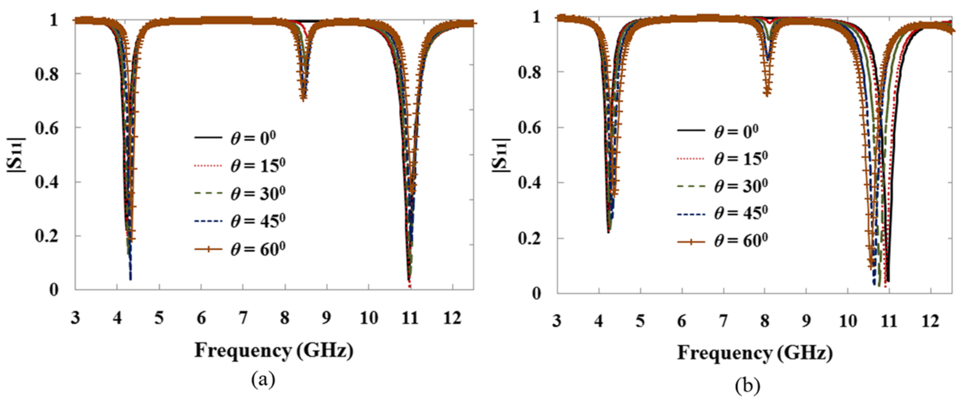

FIG. 9. Reflection characteristics under the variation of incidence angle 'θ' for (a) TE polarization, and (b) TM polarization.

proposed absorber meets the requirement of wide angle performance. A secondary resonance appears for $\theta > 0^0$ around 8.1 GHz and 8.5 GHz for the TE and TM polarized case, respectively. The H- and E-fields become inclined at an angle 'θ' for the TE and TM polarized oblique incident waves, respectively. The horizontal and vertical components of the inclined fields generate primary and secondary resonances, respectively. The horizontal component decreases with angle 'θ', and so the accumulated charge, and hence the absorption decreases with angle 'θ'. While vertical component increases with angle 'θ', and so the accumulated charge, and hence absorption increases with angle 'θ'. However, improper impedance matching is observed at the secondary resonance.

VI. CONSTITUTIVE PARAMETER RETRIEVAL

Owing to the very small thickness ($t << \lambda$) of the proposed absorber, it would be better to treat it as a metasurface. The characterization of such surfaces in terms of surface susceptibilities is the more appropriate approach compared to its characterization in terms of bulk effective material properties as discussed in Ref. 26. Moreover, this approach provides straightforward dependence of electrical surface susceptibilities (χ_{es}) and magnetic surface susceptibilities (χ_{ms}) on the S_{11} of the structure as in (4). The effective permittivity (ε_{eff}) and permeability (μ_{eff}) of the structure of thickness 't' is calculated from χ_{es} and χ_{ms} as given in (5). The applicability of these equations for such metasurfaces is already verified in Ref. 27.

$$\chi_{es} = \frac{2j}{k_0}\frac{S_{11}-1}{S_{11}+1},$$
$$\chi_{ms} = \frac{2j}{k_0}\frac{S_{11}+1}{S_{11}-1}. \tag{4}$$

$$\varepsilon_{eff} = 1 + \frac{\chi_{es}}{t},$$
$$\mu_{eff} = 1 + \frac{\chi_{ms}}{t}. \tag{5}$$

where, k_0 is wave-number of the free space.

As discussed earlier that the normalized impedance (Z) of the structure should be unity for perfect absorption. The relation of intrinsic impedance of the structure with its permittivity and permeability is given in (6). Therefore, the real and imaginary parts of ε_{eff} and μ_{eff} should be equal separately for getting perfect absorption.

$$Z(\omega) = \sqrt{\frac{\mu(\omega)}{\varepsilon(\omega)}} \tag{6}$$

where,

$$\mu(\omega) = \mu'(\omega) - j\mu''(\omega),$$
$$\varepsilon(\omega) = \varepsilon'(\omega) - j\varepsilon''(\omega).$$

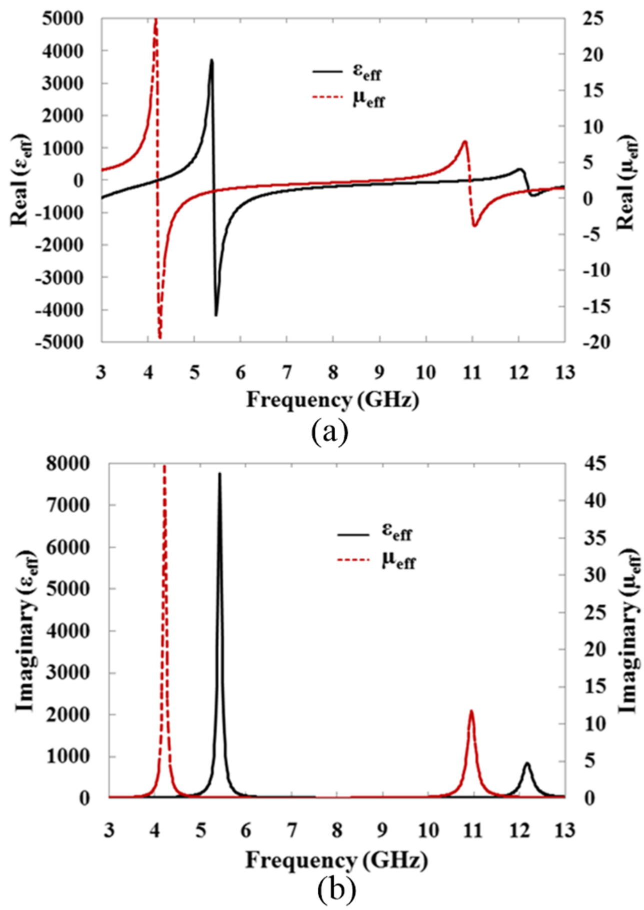

FIG. 10. Extracted constitutive parameters of the proposed structure: (a) Real part of ε_{eff} and μ_{eff}, and (b) Imaginary part of ε_{eff} and μ_{eff}.

TABLE I. Constitutive parameters of the proposed structure at the peak absorption frequencies.

Frequency (GHz)	Real (ε_{eff})	Real (μ_{eff})	Imaginary (ε_{eff})	Imaginary (μ_{eff})
4.215	1.48	-0.19	17.99	44.52
10.95	0.66	1.40	10.14	11.69

The frequency response of the extracted real part of ε_{eff} and μ_{eff} and imaginary part of ε_{eff} and μ_{eff} considering the normal incidence of the wave are presented in Fig. 10(a) and (b), respectively, and their values corresponding to the two peak absorption frequencies are reported in Table I. It is observed that the difference in real part of ε_{eff} and μ_{eff} and imaginary part of ε_{eff} and μ_{eff} at 4.215 GHz are more pronounced compared to the difference at 10.95 GHz. Hence, the extracted values further justify the low absorption at first absorption frequency compared to second absorption frequency.

VII. EXPERIMENTAL RESULTS

An array of 216 x 216 mm^2 (18 x 18 unit cells) of the proposed absorber is fabricated. Free space measurement method is employed for the measurement of the reflection response of the fabricated sample. Since the absorption response lies in C-band (4.215 GHz) and X-band (10.95 GHz), two pairs of C- and X-band horn antennas are used as transmitting and receiving antennas. The horn antennas are connected to the Anritsu's vector network analyzer MS2038C to measure S_{21}. The sample is placed at a distance calculated from Fraunhofer far field criteria. The experimental setup

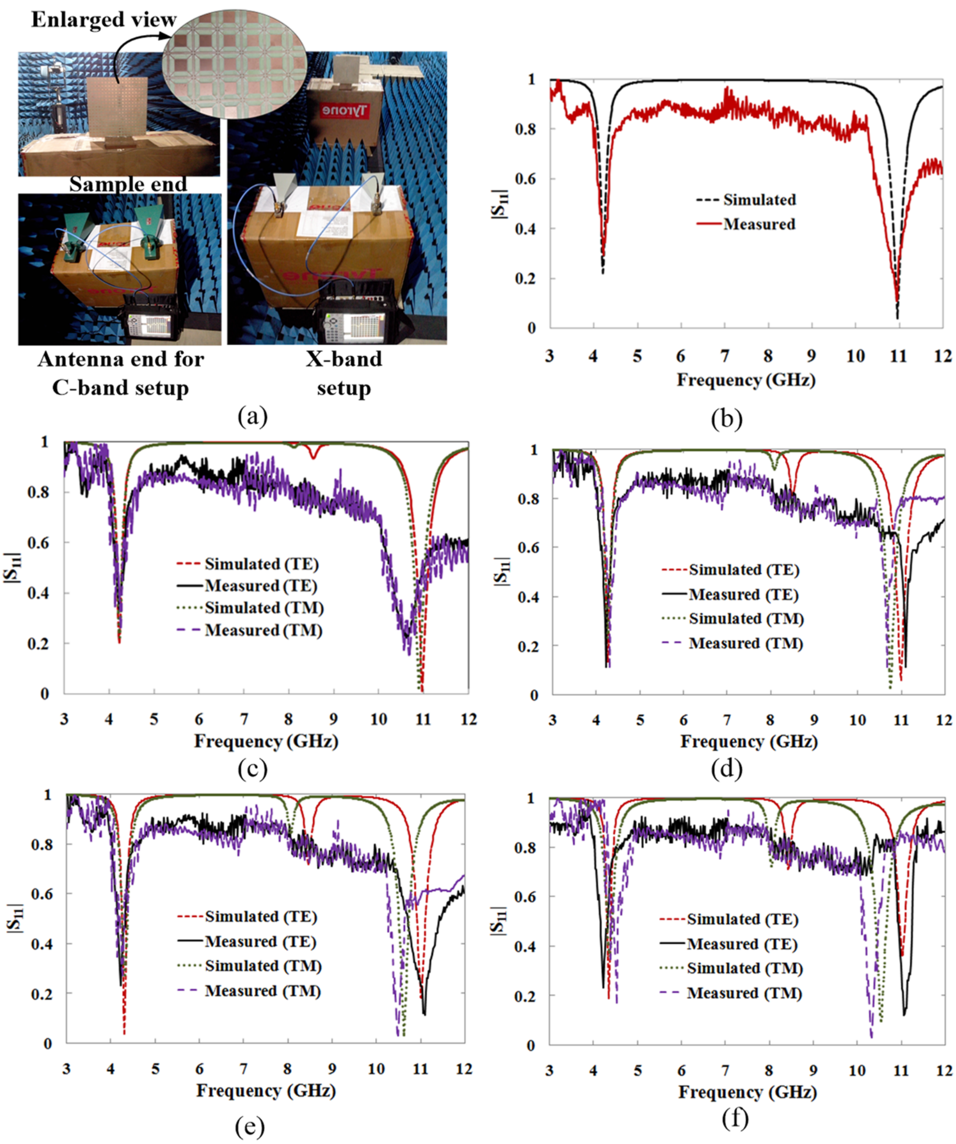

FIG. 11. (a) Experimental setup and (b) comparison of measured and simulated reflection response for normally incident wave, and oblique incidence of (c) 15^0 (d) 30^0 (e) 45^0 (f) 60^0.

in the anechoic chamber is shown in Fig. 11(a). To avoid any unwanted effect of the imperfections due to surrounding and edges/corners of the sample, the reflection from the sample are normalized with the reflection from the copper sheet of identical dimensions. The measured and simulated reflection responses of the proposed absorber for normally incident wave are compared in Fig. 11(b). The measured absorptivities of 91.30 % and 98.80 % are obtained at 4.224 GHz and 10.94 GHz, respectively. The obtained measured response is pretty close to the simulated response. The slight discrepancy in the results is due to the finite size of the fabricated sample and the fabrication tolerance of the structure. It is also observed that the measured response remains identical when we rotate the *E*-plane of both the transmitting and receiving horn antennas by 90^0 to realize TM polarized incident wave. Now the angle of the incident wave is varied from 0^0 to 15^0 by turning both the antennas by 15^0, and the measured response for the TE and TM polarized cases are compared with the simulated response in Fig. 11(c). Almost similar results are obtained at the first absorption frequency and the second absorption frequency slightly shifts from 10.965 GHz to 10.65 GHz (~2.9 %) and 10.89 GHz to 10.67 GHz (~2 %) for the TE and TM polarized case, respectively. Almost similar simulated and measured response is observed for 30^0, 45^0, and 60^0 angles of incidence and presented in

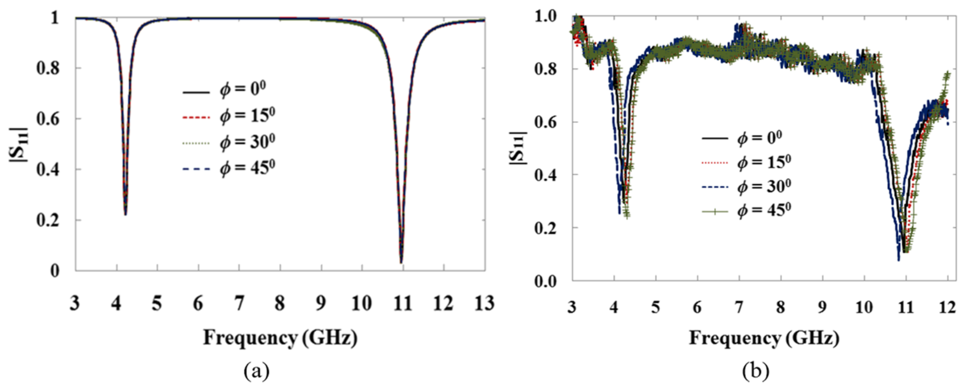

FIG. 12. (a) Simulated and (b) measured reflection response under the variation of polarization angle 'ϕ'.

TABLE II. Performance Comparison.

Reference	Peak absorption frequency and Peak absorptivity	Unit cell periodicity	Unit cell thickness
28	11.15 GHz (97%) and 16.01 GHz (99%)	12 mm (0.446λ)	0.5 mm (0.019λ)
29	6.10 GHz (98.5%) and 10 GHz (99.7%)	12 mm (0.244λ)	1 mm (0.020λ)
30	4.0 GHz (99%) and 5.6 GHz (84%)	25 mm (0.333λ)	1.6 mm (0.021λ)
31	9 GHz (97.00%) and 10 GHz (97.77%)	18 mm (0.540λ)	0.8 mm (0.024λ)
32	5.6 GHz (97%) and 6 GHz (99%)	20 mm (0.373λ)	1.5 mm (0.028λ)
33	4.42 GHz (95.6%) and 5.62 GHz (99.9%)	19.9 mm (0.293λ)	1.6 mm (0.024λ)
Proposed	4.215 GHz (95.02%) and 10.95 GHz (99.84%)	12 mm (0.169λ)	0.8 mm (0.011λ)

where λ corresponds to the lowest peak absorption frequency.

Fig. 11(d)–(f). It is also observed that the discrepancy in the measured and simulated reflection response increases with the incidence angle 'θ' and it is due to the imperfection in the placement of standard horn antennas tilted at an angle 'θ' during the experiment.

The polarization insensitive behavior of the proposed structure is investigated and presented in Fig. 12. The plane containing the *E-H* vector of the incident wave is rotated from 0^0 to 45^0 (response for the above angles will remain same owing to the diagonal symmetry in the structure). Identical reflection response is observed for the variation in polarization angle 'ϕ' (see Fig. 12(a)) and hence the proposed structure is polarization insensitive. The measured reflection response of the proposed absorber is found in good agreement with the simulated results (see Fig. 12(b)).

VIII. PERFORMANCE COMPARISON WITH SOME OTHER DUAL-BAND ABSORBERS

The comparison of the proposed absorber unit cell is presented in Table II with some other dual-band absorber structures reported in the literature.[28–33] The comparison is done in terms of unit cell periodicity and thickness. It is observed that proposed absorber is compact and ultra-thin compared to the other absorbers.

IX. CONCLUSIONS

In this paper, a single absorber unit cell with dual-band absorption response is presented. The structure is analysed parametrically and its absorption mechanism is explained. The proposed structure is polarization insensitive and is having wide angle performance for both the TE and TM polarized incident wave. Constitutive electromagnetic parameters of the structure are extracted to get an insight into the absorption phenomenon. The experimental results of the proposed absorber are found in close agreement to the simulated results. The proposed dual-band absorber structure provides the way to further realize multiband absorbers by varying the geometric parameters in the adjacent unit cells.

ACKNOWLEDGMENTS

Authors' are thankful to the Science and Engineering Research Board (SERB), New Delhi, Govt of India for providing financial support in the form of funded research project (Project No.: EEQ/2016/000744). Mayank Agarwal is thankful to University Grant Commission, New Delhi, India for providing financial assistantship in the form of Senior Research Fellowship (SRF).

[1] W. W. Salisbury, "Absorbent body of electromagnetic waves," US Patent 2 599 944, Jun. 10, 1952.
[2] R. L. Fante and M. T. McCormack, IEEE Trans. Antennas Propag. **36**(10), 1443 (1988).
[3] Y. Naito and K. Suetake, IEEE Trans. Microw. Theory Tech. **19**(1), 65 (1971).
[4] S. Sugimoto, S. Kondo, K. Okayama, H. Nakamura, D. Book, T. Kagotani, M. Homma, H. Ota, M. Kimura, and R. Sato, IEEE Trans. Magn. **35**(5), 3154 (1999).
[5] M. Park, J. Choi, and S. Kim, IEEE Trans. Magn. **36**(5), 3272 (2000).
[6] L. J. Du Toit, IEEE Antennas Propag. Mag. **36**(6), 17 (1994).
[7] H. Zhang, X.-Y. Cao, J. Gao, H.-H. Yang, and Q. Yang, Prog. Electromag. Research Lett. **44**, 35 (2014).
[8] K. Iwaszczuk, A. C. Strikwerda, K. Fan, X. Zhang, R. D. Averitt, and P. U. Jepsen, Opt. Express **20**, 635 (2012).
[9] Y. Lee, D. H. Ga, T. Song, and J. Choi, IEEE Intern. Worksh. on Ant. Tech. (iWAT), Tucson, AZ, USA, 277-280 (2012).
[10] W. Li, X. Zhou, Y. Ying, X. Qiao, F. Qin, Q. Li, and S. Che, AIP Advances **5**, 067151 (2015).
[11] N. Landy, S. Sajuyigbe, J. Mock, D. Smith, and W. Padilla, Phys. Rev. Lett. **100**(20), 207402 (2008).
[12] Y. Cheng and H. Yang, Journal of Applied Physics **108**, 034906 (2010).
[13] B. Zhu, Z. Wang, C. Huang, Y. Feng, J. Zhao, and T. Jiang, Progress in Electromagnetics Research **101**, 231 (2010).
[14] Z. X. Cao, F. G. Yuan, and L. H. Li, J. Appl. Physics **115**, 184904 (2014).
[15] Y. Q. Ye, Y. Jin, and S. He, Opt. Soc. Am. B **27**, 498 (2010).
[16] S. Bhattacharyya, S. Ghosh, and K. V. Srivastava, J. Appl. Phys. **114**, 094514 (2013).
[17] H. Tao, C. M. Bingham, D. Pilon, K. Fan, A. C. Strikwerda, D. Shrekenhamer, W. J. Padilla, X. Zhang, and R. D. Averitt, J. Appl. Phys. D **43**, 225102 (2010).
[18] Q. Y. Wen, H. W. Zhang, Y. S. Xie, Q. H. Yang, and Y. L. Liu, Appl. Phys. Lett. **95**, 241111 (2009).
[19] X. Shen, T. J. Cui, J. Zhao, H. F. Ma, W. X. Jiang, and H. Li, Opt. Express **19**, 9401 (2011).
[20] P. V. Tuong, J. W. Park, J. Y. Rhee, K. W. Kim, W. H. Jang, and H. Cheong, Appl. Phys. Lett. **102**, 081122 (2013).
[21] X.-R. Guo, Z. Zhang, J.-H. Wang, and J.-J. Zhang, J. Electromagn. Waves Appl. **27**, 629 (2013).
[22] Y. Pang, H. Cheng, Y. Zhou, and J. Wang, J. Appl. Physics **113**, 114902 (2013).
[23] K. C. Gupta, R. Garg, I. Bahl, and P. Bharti, *Microstrip Lines and Slotlines*, 2nd Edition (Artech House, Boston, 1996).
[24] F. Costa, S. Genovesi, A. Monorchio, and G. Manara, IEEE Trans. on Antennas and Propagation **61**(3), 1201 (2013).
[25] J. E. Raynolds, B. A. Munk, J. B. Pryor, and R. J. Marhefka, J. Appl. Phys. **93**, 5346 (2003).
[26] C. L. Holloway, E. F. Kuester, and A. Dienstfrey, IEEE Antennas and Wireless Propagation Letters **10**, 1507 (2011).
[27] S. Bhattacharyya and K. V. Srivastava, Journal of Applied Physics **115**, 064508 (2014).
[28] M.-H. Li, H.-L. Yang, and X.-W. Hou, Prog. Electromag. Research **108**, 37 (2010).
[29] H. B. Baskey and M. J. Akhtar, IEEE Int. Microwave RF Conf., New Delhi, India, 1–4 (2013).
[30] F. Dincer, M. Karaaslan, E. Unal, and C. Sabah, Prog. Electromag. Research **141**, 219 (2013).
[31] O. Ayop, M. K. A. Rahim, N. A. Murad, and N. A. Samsuri, Proc. of Int. Symp. Ant. and Prop. Conf., Kaohsiung, Taiwan, 195–196 (2014).
[32] S. Jamilan, M. N. Azarmanesh, and D. Zarifi, Prog. Electromag. Research C **47**, 95 (2014).
[33] F. Dincer, M. Karaaslan, E. Unal, K. Delihacioglu, and C. Sabah, Prog. Electromag. Research **144**, 123 (2014).